DOI: 10.1002/chem.201001411

In and Ex Situ Studies of the Formation of Layered Microspherical Hydrozincite as Precursor for ZnO

Marko Bitenc,[a] Peter Podbrščček,[a] Pavo Dubček,[b] Sigrid Bernstorff,[c] Goran Dražić,[d] Bojan Orel,[e] Stane Pejovnik,[f] and Zorica Crnjak Orel*[a]

Abstract: Layered ZnO microspheric particles were prepared by the thermal decomposition of layered hydrozincite (LZnHC), which was synthesized from zinc nitrate and urea in a water/PEG400 mixture. The influence of the starting reagents, their concentrations, and the amount of PEG in the water/PEG400 mixture on the particle growth was observed. The chemical aspect of the particle growth was proposed in the frame of the partial charge model (PCM), and the formation of $[Zn(OH)_2(OH_2)_4]^0$ and $[Zn(OH)(HCO_3)(OH_2)_3]^0$ was predicted for the solid phase. The assumed growth mechanism, which follows the "nonclassical crystallization" concept of a self-assembling mechanism, was observed in situ by small-angle X-ray scattering (SAXS) and predicts the rapid formation of approximately 6 nm sized building units. The size of these nano building units, stable only in the reaction medium, remains nearly constant during the synthesis, as the concentration of the nano building units increases throughout the reaction. The nano building units connect into leaves of LZnHC with a thickness of 20 nm. These leaves of LZnHC are further agglomerated into porous, microsphere-like particles with sizes up to 4 μm.

Keywords: crystal growth · hydrozincite · layered compounds · self-assembly · zinc

Introduction

Layered ZnO (LZnO) compounds have attracted increasing attention on account of their specific structure and potential applications in many areas, such as chemical sensors, photocatalysts, phosphors, and dye-sensitive solar cells.[1] Most of the LZnO particles are prepared by the thermal decomposition of the corresponding layered zinc hydroxide compounds, such as hydrozincite (zinc hydroxide carbonate, ZnHC) or zinc hydroxide acetate.

Layered zinc hydroxide carbonate (LZnHC) is commonly prepared by a solution method.[2] The hydrothermal precipitation of LZnHC from zinc nitrate with urea was already presented in our previous paper, in which the influence of the different additives on the final morphology of the particles was studied in a closed reactor system.[2a] The precipitated ZnHC decomposed in only one relatively sharp step. The decomposition activation energy of the ZnHC into ZnO was calculated on the basis of isothermal decomposition studies.

Recently, Zeng et al.[2b] used ex situ characterization (SEM and TEM) to propose the formation of LZnHC microspheres obtained by a hydrothermal process using zinc nitrate and urea in a Teflon-lined autoclave. They proposed that morphological evolution leads from a single nanosheet to dumbbell-like aggregates, which in the end formed cabbage-like spheres. Another ex situ formation of LZnHC was followed in a mixture of water and 1-butanol from zinc nitrate and urea in a Teflon-lined autoclave by Xingfu et al.[2c] They proposed a plausible dissociation–deposition mechanism for the formation of the $Zn(OH)_2$ nucleus (the "sacrifi-

[a] M. Bitenc, P. Podbrščček, Dr. Z. Crnjak Orel
Laboratory for the Spectroscopy of the Materials
National Institute of Chemistry Slovenia,
Hajdrihova 19, 1001 Ljubljana (Slovenia)
Fax: (+386) 1-476-0300
E-mail: zorica.crnjak.orel@ki.si

[b] Dr. P. Dubček
Materials Research Dept., Ruđer Bošković Institute
P.O. Box 180, 10002 Zagreb (Croatia)

[c] Dr. S. Bernstorff
Sincrotrone Trieste, S.C.p.A., 34012 Basovizza TS (Italy)

[d] Prof. Dr. G. Dražić
Department for Nanostructured Materials, Jožef Stefan Institute
Jamova 39, 1000 Ljubljana (Slovenia)

[e] Prof. Dr. B. Orel
Faculty of Computer and Information Science
University of Ljubljana, Tržaška cesta 25, 1000 Ljubljana (Slovenia)

[f] Prof. Dr. S. Pejovnik
Faculty of Chemistry and Chemical Technology
University of Ljubljana, Aškerčeva 5, 1000 Ljubljana (Slovenia)

cial" templates) for the microspherical assembly of multilayered ZnHC, thermally decomposed into LZnO.

To the best of our knowledge, only ex situ characterization methods such as TEM and SEM have been used to follow the particle growth of LZnHC.[2b,3] An ex situ observation essentially involves large time steps and a statistical uncertainty in the sampling and sample preparation. Additionally, an ex situ observation in a rigorous microscope environment can considerably alter the information about the products.

For this reason we performed an in situ measurement of the small-angle X-ray scattering (SAXS), since with this method a direct look at the growth of the nanoparticles of ZnHC was possible. In situ SAXS measurements and the growth kinetics of ZnO nanocrystals have already been presented in a series of papers.[4] However, despite an extensive search, we found no reports of in situ SAXS measurements of ZnHC growth.

To understand the formation of ZnHC, the solution chemistry of the zinc cation and the thermal decomposition of urea were considered. The solution chemistry of the zinc cation appears to be complicated, as the reactions depend on many parameters, such as the pH, the concentration, the presence of other anions, or the temperature.[5] The chemical reactions that are involved in the formation of the solid phase, such as hydrolysis, condensation, and complexation, could be discussed in the frame of the partial charge model (PCM).[6] The PCM is a simple theoretical model based on the concept of electronegativity; it provides a very useful and powerful tool to forecast the chemical behavior of an ion in solution. Other important chemical parameters, such as the pressure, ionic strength, or metal concentration, are not yet explicitly involved in the model, so the calculated structure schemes are only indicative and tentative, but still help to improve our understanding of the system.

The influence of different polyols such as ethylene glycol, diethylene glycol, and tetraethylene glycol on the morphology of the final particles of the ZnO was presented in our previous paper.[7] ZnO, in the form of hexagonal bipods, was synthesized from zinc nitrate and urea in an open reactor with constant stirring in a one-step reaction (no additional treatment was necessary). We found that the particles were more homogenous and stable when a mixture of water and a different polyol was used. In a series of papers, the preparation of one-dimensional ZnO nanostructures in water solutions with addition of different long- and short-chain polymers has been reported.[8] For instance, Li et al.[8f] used a short-chain polymer such as polyethylene glycol 400 (PEG400) for the fabrication of ZnO particles in a one-step reaction. They showed that synthesized nanoparticles could be selectively prepared by using short-chain polymers.

In this work we present the preparation of LZnHC from zinc nitrate and urea in a water and a water/PEG mixture in an open reactor with constant stirring. The growth of the microspheric LZnHC precursor, which was thermally decomposed into LZnO, was followed with in situ SAXS measurements and both field-emission scanning electron microscopy (FESEM) and TEM. To understand the different growth mechanism and kinetics, various concentrations of starting reagents were used in the mixed solution of water and a different volume ratio of PEG400. The formation mechanism of the LZnHC, formed in the water/PEG mixture, as observed from the SAXS data and theoretically calculated by PCM, is presented in this paper for the first time.

Results and Discussion

Thermal decomposition of urea and the formation of the ZnHC: Layered hydrozincite (LZnHC) was synthesized from zinc nitrate and urea in the water and the water/PEG400 mixture. For a better understanding of the growth of the ZnHC particles during the precipitation, the decomposition of urea needs to be taken into account. The decomposition of urea depends on the experimental conditions such as the temperature, the time of synthesis, and the pH, as the system is very sensitive to any changes.[9] We can summarize that a number of cations and anions, such as the oxonium and ammonium cations and hydroxide, carbonate, hydrogen carbonate, and cyanate anions, were formed, depending on the experimental conditions. However, in this rather complicated decomposition, there are also carbon dioxide and ammonia gases. Investigations of the decomposition of urea in a water medium, presented by Matijević and Sapieszko,[9a] showed that the decomposition increases with a rise in temperature. They reported that urea degradation takes place 25 times faster at 90 °C than at 60 °C. It is also known that the presence of metal ions such as zinc catalyze the urea decomposition and consequently the mechanism of decomposition could be modified, shortened, and more complex.[9b]

The pH of the solution was measured during the synthesis to observe the chemical behavior of our system (Figure 1). The pH measurement of the thermal decomposition of urea (0.5 M) in water is presented in Figure 1a. From the pH values the pH drop could be seen in the first 10 min. When the final temperature (90 °C) of our system was reached (after 15 min of the reaction) urea began to decompose faster. The pH of the solution increased subsequently to a

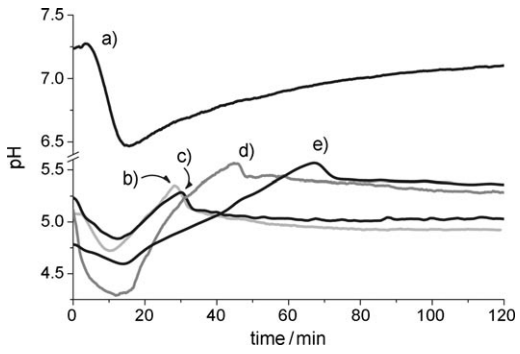

Figure 1. pH as a function of time of a) urea (0.5 M) thermal decomposition in water, b) Sample I, c) Sample IV, d) Sample III, and e) Sample II.

pH value of around 7 after 2 h of decomposition. Similar pH curves were obtained for the thermal decompositions of urea in water/PEG400 mixtures (not presented in the paper).

In Figure 1b, the pH measurement of the synthesis in the water medium (Sample I, Table 1) is presented and the pH measurements of water/PEG400 mixture at volume ratio of 3:1 (listed in Table 1) are presented in Figure 1c–e. The shapes of the pH curves of the experiments in the water/PEG400 mixtures (Figure 1c–e) were very similar to those obtained in the water medium (Figure 1b). For that reason, the chemical formation of the solid phase in the water/PEG mixture is predicted to be analogous to the synthesis in the water medium.

Table 1. Experimental conditions for the preparation of the samples and the time of the formation of the particles obtained by SAXS, FESEM, and pH measurements.

Sample	Vol. ratio of water/PEG400	Zn^{2+} [M]	Time of particle formation [min]	
			SAXS	SEM/pH
I	1:0	0.1	26	29
II	3:1	0.025	73	70
III	3:1	0.05	42	45
IV	3:1	0.1	25	28
V	1:1	0.025	112	108
VI	1:1	0.05	49	55
VII	1:1	0.1	37	35

The theoretical formation of the solid compounds from solution was based on the hydrolysis, condensation, and complexation reaction of the zinc cation in the framework of the partial charge model (PCM). The PCM is based on the electronegativity equalization that allows for an estimation of the charge and the identification of the molecular species of cations at specific values of pH.

In the very beginning of our synthesis, the zinc nitrate was in the form of a fairly stable hydrated zinc, in which zinc cations are octahedrally coordinated in the form of the hexaqua $[Zn(OH_2)_6]^{2+}$ and hydroxo–aquo complex $[Zn(OH)(OH_2)_5]^{+}$.[10] The hydroxo–aquo complexes existed when the hydrolysis ratio (h) was 1.3, calculated with the PCM for an initial pH 5. The hydrolysis ratio (h) corresponds to the number of protons that have been removed from the metal–aqua complex and increases along with the pH.[6a] During the hydrolysis of the Zn^{2+} cation, the pH value in the reaction medium was decreased.

With a gradual increase in temperature up to 90 °C during the first 15 min of the synthesis, the pH of the reaction medium subsequently increased (Figure 1b–d) due to the faster decomposition of the urea. The numerically solved thermal decomposition of the urea in water at 80 °C shows that ammonium, cyanate, and hydrogen carbonate are among the most relevant species during the urea decomposition.[9b]

The cyanate anion could be catalytically hydrolyzed by the zinc ion, so the aqua ligand in a zinc hydroxo–aquo complex is deprotonated into a hydroxo ligand, and ammonium and hydrogen carbonate are formed.[9b] The reaction can be written as follows [Eq. (1)]:

$$[Zn(OH)(OH_2)_5]^{+} + OCN^{-} + 2\,H_2O \rightarrow [Zn(OH)_2(OH_2)_4]^{0} + NH_4^{+} + HCO_3^{-} \quad (1)$$

With this reaction, we could explain the neutralization of the divalent zinc ion in an aqueous solution, in which $h=2$ is needed. The upper limit of our hydrolysis ratio was 1.5, calculated by PCM for pH 5.7, which was the maximum measured pH value in our reactions.

With the PCM model, we would be able to explain the complexation behavior of the anionic species towards the aqueous Zn^{2+} precursor.[5] In our case, the zinc aqueous precursor could be complexed by monovalent anions (X^{-}) such as HCO_3^{-} and NO_3^{-}. Our reaction system could be then written as follows [Eq. (2)]:

$$[Zn(OH)(OH_2)_5]^{+} + X^{-} \leftrightarrow [Zn(OH)(X)(OH_2)_{5-\alpha}]^{0} + \alpha H_2O \quad (2)$$

in which α corresponds to the number of water molecules that are replaced by the anion X^{-}. According to the literature, the HCO_3^{-} and NO_3^{-} anions behave as bidentate ligands ($\alpha=2$) and should be able to replace two water molecules.[6a] The stability of the Zn−X complex with respect to ion dissociation and hydrolysis could be calculated by the PCM. We determined that $[Zn(OH)(HCO_3)(OH_2)_3]^{0}$ was the only stable complex under our experimental conditions ($h=1$), as the NO_3^{-} anion, due to its high electronegativity, is dissociated.

It is known that the presence of the $[Zn(OH)_2(OH_2)_4]^{0}$ and $[Zn(OH)(HCO_3)(OH_2)_3]^{0}$ complexes consequently lead to fast olation, which is the formation of the hydroxo or "ol" bridges and the elimination of water.[6a,11] The reaction of olation can be written as follows [Eq. (3)]:

$$3[Zn(OH)_2(OH_2)_4]^{0} + 2[Zn(OH)(HCO_3)(OH_2)_3]^{0} \rightarrow [Zn_5(OH)_6(CO_3)_2] + 20\,H_2O \quad (3)$$

The reactions gradually lead to the formation of a laminar zinc hydroxide carbonate network with a rapidly reduced solubility (critical limiting supersaturation) and further particle growth of the ZnHC. At this point, the highest pH value was measured and followed by a small decrease of the pH value as the consequence of the partial relief of the ZnHC precipitation (Figure 1b–e).[12] The reaction mixtures were in chemical equilibrium after the rapid self-nucleation, which results in the nearly constant pH value thought the reaction.

The structure of ZnHC is composed of parallel sheets of zinc in both the octahedral and tetrahedral coordinations in the ratio 3:2 (Figure 2).[13] The parallel sheets are held to-

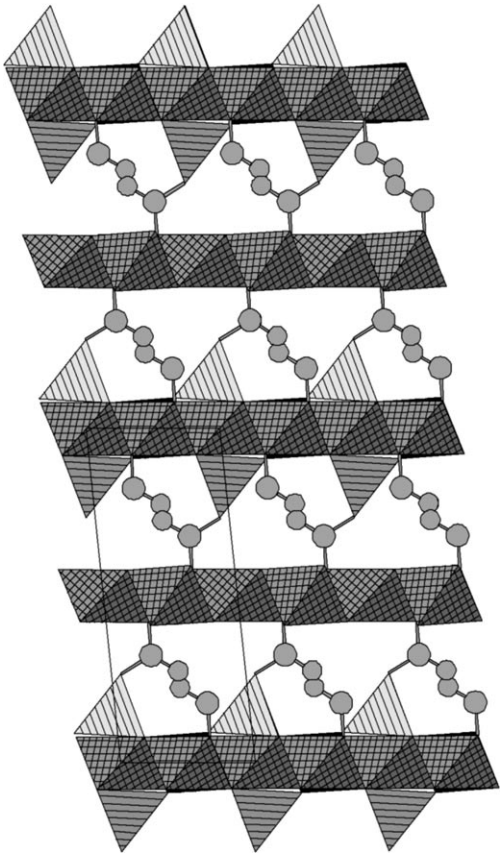

Figure 2. Crystal structure of ZnHC.

gether by a CO_3 group that is normal to the sheets. Two oxygen atoms of the CO_3 group are each bonded to an octahedral and tetrahedral zinc atom, whereas the third oxygen atom is hydrogen-bonded to three OH groups. The as-prepared ZnHC also contains water adsorbed onto the surface. Some part of the water that is present could be structural and located between parallel sheets and carbonate groups.

In situ SAXS analysis: The nucleation and growth of the particles was observed in situ by SAXS. Figure 3 presents an example of an SAXS measurement (Sample II, Table 1) for which the SAXS intensity is plotted versus the scattering vector, S, in which $S=(2\sin\theta)\lambda^{-1}$, θ is the scattering angle, and λ is the wavelength. It is clear that the particles start to form after approximately 40 min, as indicated by the arrow in Figure 3.

The SAXS intensity is a result of the interference of the waves scattered from each electron in the particle. It can be shown that the central part of the intensity (the smallest scattering angles) is similar for different shapes of the scattering particles (intensity $(I)\approx\exp[-(SR_G)^2]$). Furthermore, its dependence on the angle is given only by the size of the particle, represented by the radius of gyration, R_G.[14] The latter is defined as the mean square distance (RMS) from the center of gravity. Therefore, R_G is an intuitive measure of the spatial extension of the scattering structures. It is calculated from the slope of the scattering curve in the so-called "Guinier-plot", in which the logarithm of the scattering intensity is plotted against S^2 The Guinier approximation was derived for dilute systems and is valid in the range of small values of the scattering vector S in which the criterion $R_{G,max}q \ll 1$ $(q=2\pi/S)$ is fulfilled. It is straightforward to show that, for example, for the sphere $R_G^2=3/5R^2$, for which R is the radius of the sphere.

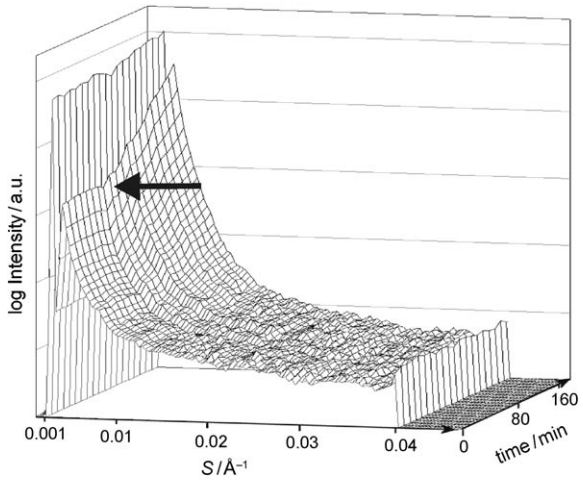

Figure 3. Logarithmic plots of the SAXS intensity versus the scattering vector (S) measured in situ during the preparation of Sample II.

The SAXS data are presented as the time evolution of the integral intensity (Figure 4) and the average size of the nanoparticles (Figure 5) for the synthesis in the water medium, and at different water-to-PEG400 volume ratios (3:1 and 1:1) in the initial solution reaction mixture. The SAXS scattering was followed in situ from the beginning of the synthesis so as to study the full range of particle formation. The intensity integration was made over 120 s to obtain an adequate signal-to-noise ratio, and this represents the time resolution of the experiment. In the beginning of the reaction, the sample scattering is equal to the solvent scattering, and this is taken as a reference. Only when the

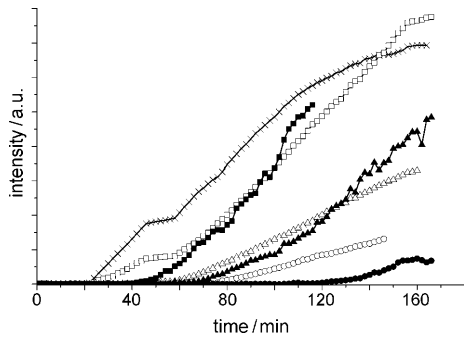

Figure 4. The integral scattering intensity versus reaction time for synthesis in water medium (Sample I: ×), 3:1 ratio (v/v) of water/PEG400 (Sample II: ○; Sample III: △; Sample IV: □), and 1:1 ratio (v/v) of water/PEG400 (Sample V: ●; Sample VI: ▲; Sample VII: ■).

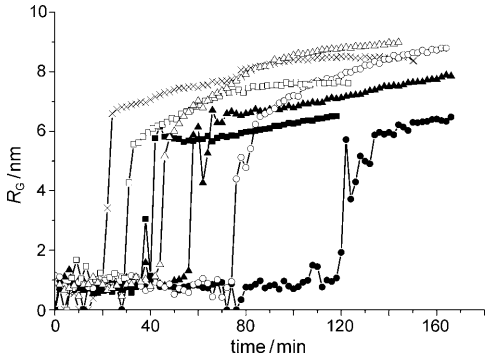

Figure 5. The R_G radius versus reaction time for synthesis in water medium (Sample I: ×), 3:1 ratio (v/v) of water/PEG400 (Sample II: ○; Sample III: △; Sample IV: □), and 1:1 ratio (v/v) of water/PEG400 (Sample V: ●; Sample VI: ▲; Sample VII: ■).

particles start to form does the SAXS begin to change. In the first 20 min of the reaction the formation of the particles was not expected since the thermal decomposition of the urea was slow at the beginning of the synthesis and subsequently the appropriate formation of the $[Zn(OH)_2(OH_2)_4]^0$ and $[Zn(OH)(HCO_3)(OH_2)_3]^0$ complexes needed for the nucleation were not possible.

The change of the SAXS integral intensity as a function of time serves as a good measure for the amount of formed material. In the beginning of the synthesis, the SAXS intensity increases as a square of the time. We can determine the moment at which the particles start to form in the solution by extrapolating the square function fitted to the data in Figure 4 to zero. The moment when the formation of the particles begins, given by the square fit of the initial growth, is presented in Table 1.

The formation of the particles started faster for higher concentrations of the initial reagents (Table 1). Experiments with the same concentration of the initial reagents, but with a higher volume ratio of PEG400 used in the water/PEG400 mixture, showed that larger amounts of PEG400 retard the formation rate of the nanoparticles in the beginning of the synthesis. After a certain period, depending on the concentrations of the initial reagents, the intensity increase with time changes to a linear mode. In the first group of samples (water and water/PEG400 at a 3:1 v/v ratio, presented in Figure 4), the SAXS intensity grows linearly with time, almost immediately after the initial moment of formation. The changeover to the linear mode happens later for the second group of samples (water/PEG400 ratio was 1:1 v/v), as presented in Figure 4. An explanation can be found in the assumption that the larger amount of PEG400 influences the formation of the microenvironment. We can propose that the chainlike PEG molecules segmented the open linear reaction field in which complexation of the zinc cation was limited at the beginning of the synthesis (square function) and later became constant (linear function).[15]

The Guinier[14] approximation was used to follow the typical size evolution with time. The obtained Guinier radii (R_G) are plotted as a function of time in Figure 5. For the all experiments, an abrupt particle formation about 6 nm in size can be observed (Figure 5) when the particles start to grow. The size of the particles tends to saturate towards the end of the particle growth and does not exceed 10 nm for the particles in water medium (Sample I, Figure 5), and 9 and 8 nm for the particles in water/PEG400 mixture with ratios of 3:1 and 1:1 (v/v), respectively. The Guinier radii of the particles decreases with the increased amount of the PEG400 in the reaction mixture. The growth of the ZnHC particles was most sluggish in a case of Sample V, for which the lowest concentration of the initial reagent was used in the mixture of water/PEG400 with ratio of 1:1 (v/v) and the fastest in Sample I for which a pure water medium was used (Figure 5). We can see in Figure 5 that a typical size of 6 nm is reached within two minutes after the beginning of the process for all samples with the exception of Sample I.

Ex situ FESEM and TEM analysis: Detailed FESEM and TEM analyses were performed to completely understand the time-dependent growth of the particles. The formation time of the first particles synthesized in water and in water/PEG400 mixtures with a ratio of 3:1 and 1:1 (v/v), observed by FESEM (micrographs not presented in the paper), agrees well with the time determined by the SAXS, as presented in Table 1.

The detailed time-dependent growth of the particles, after the first observation with FESEM and TEM, is described for Sample IV (Table 1, Figure 6). However, the other samples show a similar growth behavior to that presented for Sample IV. From the FESEM image of Sample IV (Figure 6a1), it is clear that the obtained layered particles are difficult to distinguish. On the other hand, one can see the groups of organized crystal planes with a size of around 5 nm (Figure 6a2), which are incorporated into the leaflike matrix of ZnHC. The selected-area electron diffraction (SAED) pattern (not presented in the paper) shows that the particles are randomly oriented and extremely small.

Our tentative explanation for the growth mechanism proposes that the nanoparticles (building units around 5 nm in size) were self-assembling into a growing, microscopic ZnHC crystal network (Figure 6a2). At the same time, new nanoparticles were forming. The particle-mediated growth through a self-assembly mechanism is part of the "nonclassical crystallization" concept, which is not new.[12,16] However, we show with these results, to the best of our knowledge, the first proof of a nonclassical crystallization growth behavior for this system.

The first microspherical particles with an estimated size up to 2 μm were observed after 30 min of the reaction (Figure 6b1). The spheres are composed of sheets with a thickness of around 20 nm (Figure 6b2). Approximately 6 nm large crystallites could be observed in the obtained structures (Figure 6b2, inset; high-resolution transmission electron microscopy (HRTEM)). For the same reaction time, the SAXS data showed the presence of nanoparticles approximately 6 nm in size. On the other hand, individual

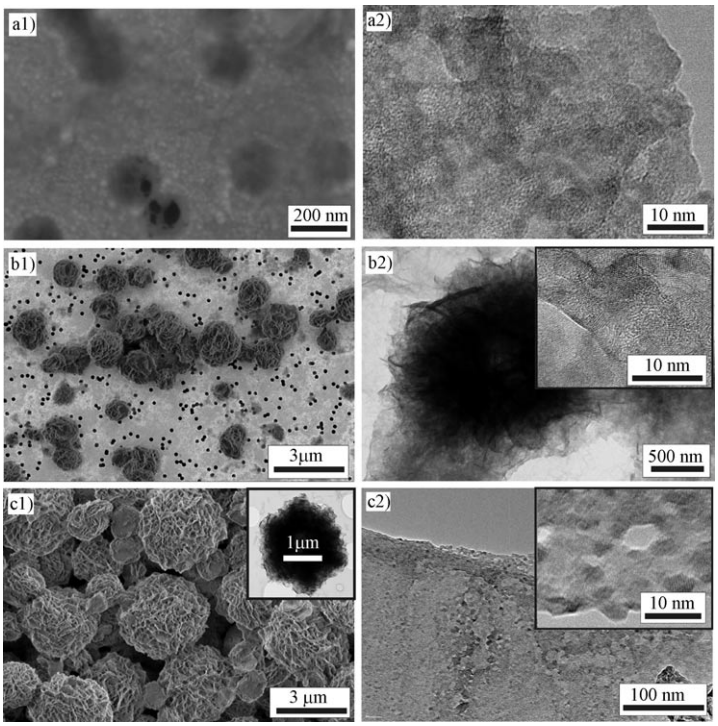

Figure 6. FESEM and TEM micrographs of Sample IV (Table 1) prepared after a) 28, b) 30, and c) 32 min.

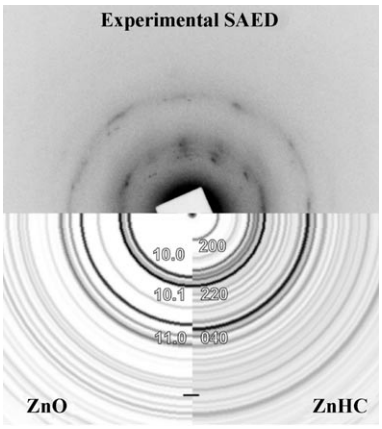

Figure 7. Experimental SAED pattern of Sample IV obtained after 35 min of the synthesis and comparison with simulated patterns of ZnO and ZnHC.

nanoparticles (separated from the solution and larger particles) were not detected by (ex situ) SEM and TEM microscopy, so we suppose that they were only stable in the reaction system.

After 32 min of the reaction, the concentration of the spherelike particles had rapidly increased (Figure 6c). The size of the porous microsphere-like particles was between 1 and 4 μm (Figure 6c1). From the TEM image it can be observed that leaves, with a thickness around 20 nm, composed the spherelike particles in a three-dimensional hexagonal order (Figure 6c1, inset). Our mechanism predicts the agglomeration of separate leaves into larger, porous microsphere-like particles with subsequent growth. The HRTEM image of the individual leaf, presented in Figure 6c2, shows that the leaves were formed of nanoparticles that were approximately 6 nm in size (Figure 6c2, inset). According to the SAXS data, the sizes of the nanoparticles in the reaction medium were still nearly constant. From the SAED pattern of this sample it could be observed that the particles are very small (diffuse circles) and randomly oriented (uniform circles). From a comparison of the experimental and simulated SAED patterns (the EMS computer program was used for the simulation[17]), presented in Figure 7, it was found that these nanocrystals are mainly composed of hydrozincite. The sample was found to be relatively sensitive to irradiation with the electron beam, and this was reason why some evidence for ZnO was also observed (Figure 7).

Additionally, we found that the formation of the particles could be followed simply by the pH measurement during the synthesis (Figure 1b–e). The time at which the measured pH reached the highest value was in good agreement with the time when the first particle formation was observed with the electron microscopy. The samples prepared in water and water/PEG400 at ratios of 3:1 and 1:1 (v/v) showed that the formation of the particles obtained by SAXS and the agglomeration of the particles presented by FESEM were closer to each other, which is in agreement with the time at which the highest pH was measured. From these observations, the pH measurements were found to be a useful tool to control the formation of the particles in our experiments.

Formation of ZnO: To produce pure ZnO, the samples were thermally treated at 300 °C for 4 h under a static atmosphere of air. The particles kept their morphology on the microscale during the heat treatment, as presented in Figure 8. However, the annealation caused the formation of a nanoporous structure on the surface of the particles (Figure 8a), which revealed an increased specific surface area.[2a]

The obtained products were also characterized with XRD and FTIR spectroscopy. For example, the XRD spectra of Sample IV are presented in Figure 9 before and after the thermal decomposition. The major peaks of the spectrum before heat treatment (Figure 9b) correspond to $[Zn_5(OH)_6(CO_3)_2]$ (powder diffraction file (PDF) 19-1458, ZnHC). From the high background and the low intensity of the peaks, it is apparent that the product is not well crystallized. In the XRD pattern of Sample IV (Figure 9b), the peak intensities of (002) are slightly higher than that of the standard pattern (PDF 19-1458). These results indicate that the leaflike particles that compose the microspheres have a pronounced dimension of (002) in the XRD pattern. This could be connected with the results presented in the paper by Hosono et al.,[1] in which they named the layered hydroxide zinc carbonate sheets, and in which leaflike samples prepared on a glass substrate show higher peak intensity of (020). For this reason we can conclude that the more pronounced peak intensity of (002) is connected with the mor-

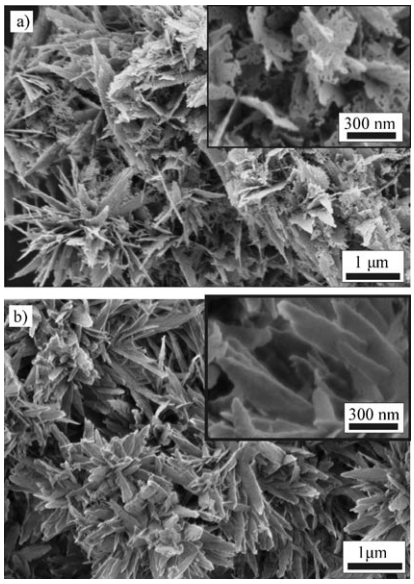

Figure 8. FESEM micrograph of Sample IV (Table 1) obtained after 2 h of synthesis a) with an additional heat treatment at 300 °C for 4 h and b) as-prepared.

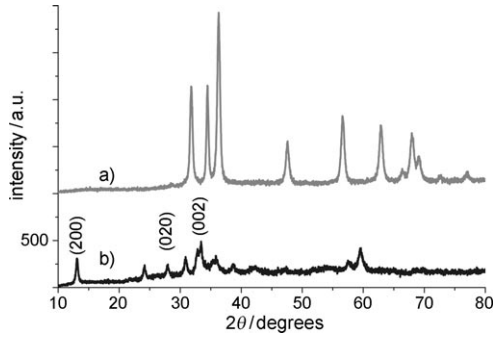

Figure 9. XRD spectra of Sample IV (Table 1) prepared after 2 h of synthesis a) after heat treatment, and b) as-prepared.

phology of the samples, because the leaflike particles that formed microspheres are wider. With thermal decomposition (300 °C) in air, the sample was transformed into a pure hexagonal ZnO phase (PDF 36-1451). The XRD pattern of that sample is shown in Figure 9a.

The FTIR spectrum of Sample IV is presented in Figure 10. The presence of CO_3^{2-} in the product was confirmed by the bands in the range from 1600 and 1200 cm^{-1}, and from 1000 to 680 cm^{-1} (Figure 10b).[2a] The FTIR spectra of the other samples (not presented in the paper) show comparable spectra. No peak corresponding to PEG in the FTIR spectrum was observed, although it is known that PEG can be easily adsorbed at the surface of a metal-oxide colloid.[8b] After a thermal treatment (300 °C) of the precipitate, the band at 429 cm^{-1} with a pronounced shoulder at 542 cm^{-1} in the IR spectra (Figure 10a) confirmed the presence of ZnO.

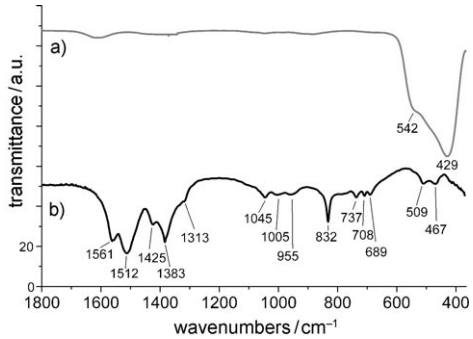

Figure 10. FTIR spectra of Sample IV (Table 1) prepared after 2 h of synthesis a) after heat treatment and b) as-prepared.

Conclusion

In this paper, we proposed the chemical aspects of ZnHC particle growth, in which the hydrolysis, condensation and complexation reactions of the zinc cation were presented in the frame of the partial charge model (PCM). With this model we explained the formation of the $[Zn(OH)_2(OH_2)_4]^0$ and $[Zn(OH)(HCO_3)(OH_2)_3]^0$ complexes, which are necessary for olation and consequently for the formation of a laminar zinc hydroxide carbonate in the form of nanoparticle building units of approximately 6 nm in size. The formation of the particles in the water/PEG mixture was found to be very rapid. However, larger amounts of PEG400 postpone the formation of the building units of the nanoparticles. We supposed that the building units of the nanoparticles were stable, individually, only in the reaction solution. The nano building units further self-assembled into leaves of ZnHC with a thickness around 20 nm. The leaves were agglomerated into porous, microsphere-like particles with sizes that ranged from 1 to 4 μm. The size of the nanoparticles remained nearly constant during the synthesis.

Experimental Section

Materials: The chemicals were analytically pure. Solutions prepared from $Zn(NO_3)_2 \cdot 6H_2O$ (Aldrich) and urea (Aldrich) in Milli-Q (Millipore) water were used. The initial concentrations of the Zn^{2+} ions and the urea were from 0.025 to 0.1 M and from 0.125 to 0.5 M, respectively. The concentration of the urea was five times higher than that of the Zn^{2+} in all the experiments. As solvents, mixtures of water and polyethylene glycol (PEG400, Merck) were used. The detailed experimental conditions for the preparation of the samples are given in Table 1.

Synthesis: The experimental setup consisted of an open reactor (250 mL) with constant stirring, which was connected by tubing and a peristaltic pump into a closed, recyclable loop. The temperature was controlled with a thermostatic bath. The reaction was started by initiating the appropriate amount of regents and media into a preheated reactor, in which the total volume of the solution was 200 mL. Volume ratios of 3:1 and 1:1 for the water/polyol mixtures were employed in the experiments. The experimental setup is schematically presented in Figure 11. Immediately after initiation the solution started pumping through the closed cycle. The temperature of the reaction mixture was increased to 90 °C. The products were filtered, washed with Milli-Q water, and dried in air at

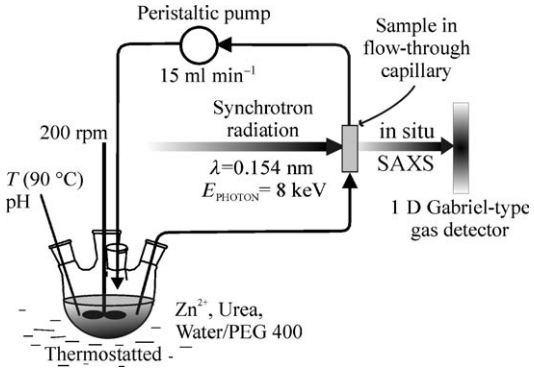

Figure 11. Schematic description of the mixing-batch reactor setup.

room temperature. To obtain zinc oxide, the products were heat-treated in an oven at 300 °C for 4 h under a static atmosphere of air.

Characterization: The reaction processes and the particle evolution were followed in situ by SAXS and by using a 1.5 mm flow-through quartz capillary (Figure 11). The SAXS experiment was carried out at the synchrotron facilities of Elettra, Trieste, Italy on the SAXS beamline, by using synchrotron radiation with wavelength $\lambda = 0.154$ nm (photon energy of 8 keV).[18] A linear position-sensitive 1D Gabriel-type gas detector, positioned perpendicular to the incident beam at a detector-to-sample distance of 2 m, was used to record the SAXS intensity. The spectra were corrected for the background intensity and the detector response. pH measurements were made in situ using a Mettler Toledo 1140 pH meter with the Mettler Toledo InPro4800/225/Pt1000 electrode. Prior to the measurement, the electrode was calibrated using a two-point calibration with the Mettler-Toledo technical buffers 4.01 and 7.00. The structures of the samples were studied using Jeol 2010 FEG STEM and Jeol 2100 TEM microscopes operating at 200 kV equipped with EDX detectors for the compositional analyses. In the case of small particles (up to 100 nm), a fraction of the particles in the form of a suspension in ethyl alcohol was transferred to a lacey carbon-coated Ni grid and examined with the microscope. High-resolution TEM (HRTEM), selected-area electron diffraction (SAED), and convergent-beam electron diffraction (CBED) were employed to examine the structures of the materials. Simulated CBED patterns, used for the polar-axis orientation, were calculated with the EMS program code.[17] The morphology and growth of the particles were characterized using scanning field-emission electron microscopy (FESEM, Zeiss Supra 35 VP with an EDS analyzer). For the FESEM observation, approximately 2 mL of the suspension was taken from the reactor, filtered off on 200 nm filter paper (Millipore, previously covered with Au), washed, and dried in air at room temperature. X-ray diffraction analyses (XRD) were carried out using a Siemens D-500 X-ray diffractometer. IR spectra were obtained using an FTIR spectrometer (Perkin–Elmer 2000) in the spectral range between 4000 and 400 cm^{-1} with a spectral resolution of 4 cm^{-1} in the transmittance mode. The KBr pellet technique was used for the sample preparation.

Acknowledgements

The authors gratefully acknowledge the financial support of the Ministry of Higher Education (project Novapol of MNT-ERA.NET), the Science and Technology of the Republic of Slovenia, and the Slovenian Research Agency (programme P1-0030).

[1] E. Hosono, S. Fujihara, I. Honna, H. S. Zhou, *Adv. Mater.* **2005**, *17*, 2091–2098.
[2] a) M. Bitenc, M. Marinsek, Z. C. Orel, *J. Eur. Ceram. Soc.* **2008**, *28*, 2915–2921; b) X. Y. Zeng, J. L. Yuan, L. Zhang, *J. Phys. Chem. C* **2008**, *112*, 3503–3508; c) X. F. Zhou, Z. L. Hu, Y. Q. Fan, S. Chen, W. P. Ding, N. P. Xu, *J. Phys. Chem. C* **2008**, *112*, 11722–11728; d) P. Podbrscek, Z. C. Orel, J. Macek, *Mater. Res. Bull.* **2009**, *44*, 1642–1646; e) C. L. Yan, D. F. Xue, *J. Phys. Chem. B* **2006**, *110*, 11076–11080; f) S. D. Skapin, G. Drazic, Z. C. Orel, *Mater. Lett.* **2007**, *61*, 2783–2788; g) B. Su, M. Li, Z. Y. Shi, Q. H. Lu, *Langmuir* **2009**, *25*, 3640–3645; h) B. Bems, M. Schur, A. Dassenoy, H. Junkes, D. Herein, R. Schlogl, *Chem. Eur. J.* **2003**, *9*, 2039–2052.
[3] X. F. Zhou, D. Y. Zhang, Y. Zhu, Y. Q. Shen, X. F. Guo, W. P. Ding, Y. Chen, *J. Phys. Chem. B* **2006**, *110*, 25734–25739.
[4] a) R. Viswanatha, H. Amenitsch, D. D. Sarma, *J. Am. Chem. Soc.* **2007**, *129*, 4470–4475; b) K. Biswas, B. Das, C. N. R. Rao, *J. Phys. Chem. C* **2008**, *112*, 2404–2411; c) M. S. Tokumoto, S. H. Pulcinelli, C. V. Santilli, A. F. Craievich, *J. Non-Cryst. Solids* **1999**, *247*, 176–182.
[5] H. Marc in *Handbook of Organic–Inorganic Materials and Nanocomposites, Vol. 1* (Ed.: H. S. Nalwa), American Scientific Publisher, Stevenson Ranch, **2003**, pp. 1–16.
[6] a) J. Livage, M. Henry, C. Sanchez, *Prog. Solid State Chem.* **1988**, *18*, 259–342; b) J. Livage, *Catal. Today* **1998**, *41*, 3–19.
[7] M. Bitenc, Z. C. Orel, *Mater. Res. Bull.* **2009**, *44*, 381–387.
[8] a) M. Bitenc, P. Podbrscek, Z. C. Orel, M. A. Cleveland, J. A. Paramo, R. M. Peters, Y. M. Strzhemechny, *Cryst. Growth Des.* **2009**, *9*, 997–1001; b) J. P. Liu, X. T. Huang, Y. Y. Li, Q. Zhong, L. Ren, *Mater. Lett.* **2006**, *60*, 1354–1359; c) J. P. Liu, X. T. Huang, *J. Solid State Chem.* **2006**, *179*, 843–848; d) C. W. Cheng, G. Xu, H. Q. Zhang, Y. Luo, P. G. Zhang, K. Shen, *Mater. Res. Bull.* **2008**, *43*, 3506–3513; e) X. M. Hou, F. Zhou, B. Yu, W. M. Liu, *Mater. Lett.* **2007**, *61*, 2551–2555; f) Z. Q. Li, Y. J. Xiong, Y. Xie, *Inorg. Chem.* **2003**, *42*, 8105–8109; g) X. X. Shi, L. L. Pan, S. P. Chen, Y. Xiao, Q. Y. Liu, L. J. Yuan, J. T. Sun, L. T. Cai, *Langmuir* **2009**, *25*, 5940–5948.
[9] a) E. Matijević, R. S. Sapieszko in *Fine Particles: Synthesis, Characterization and Mechanism of Growth* (Ed.: T. Sugimoto), Marcel Dekker, New York, **2000**, pp. 386–395; b) G. J. A. A. Soler-Illia, M. Jobbágy, R. J. Candal, A. E. Regazzoni, M. A. Blesa, *J. Dispersion Sci. Technol.* **1998**, *19*, 207–228; c) C. L. Yan, D. F. Xue, *J. Phys. Chem. B* **2006**, *110*, 7102–7106.
[10] a) A. Kawska, P. Duchstein, O. Hochrein, D. Zahn, *Nano Lett.* **2008**, *8*, 2336–2340; b) D. Kisailus, B. Schwenzer, J. Gomm, J. C. Weaver, D. E. Morse, *J. Am. Chem. Soc.* **2006**, *128*, 10276–10280.
[11] M. Henry, J. P. Jolivet, J. Livage, *Struct. Bonding (Berlin)* **1992**, *77*, 153–206.
[12] F. C. Meldrum, H. Colfen, *Chem. Rev.* **2008**, *108*, 4332–4432.
[13] S. Ghose, *Acta. Cryst.* **1964**, *17*, 1051–1057.
[14] A. Guinier, G. Forurnet, *Small-Angle Scattering of X-rays*, Chapman and Hall, London, **1955**, pp. 126–160.
[15] Z. H. Kang, E. B. Wang, M. Jiang, S. Y. Lian, Y. G. Li, C. W. Hu, *Eur. J. Inorg. Chem.* **2003**, 370–376.
[16] a) H. Zhang, E. W. Edwards, D. Wang, H. Mohwald, *Phys. Chem. Chem. Phys.* **2006**, *8*, 3288–3299; b) I. Sevonkaev, E. Matijevic, *Langmuir* **2009**, *25*, 10534–10539; c) G. Begum, S. V. Manorama, S. Singh, R. K. Rana, *Chem. Eur. J.* **2008**, *14*, 6421–6427.
[17] P. A. Stadelmann, *Ultramicroscopy* **1987**, *21*, 131–145.
[18] H. Amenitsch, S. Bernstorff, P. Laggner, *Rev. Sci. Instrum.* **1995**, *66*, 1624–1626.

Received: May 21, 2010
Published online: August 19, 2010

